Pertanika J. Trop. Agric. Sci. 48 (6): 2087 - 2117 (2025)

TROPICAL AGRICULTURAL SCIENCE

Journal homepage: http://www.pertanika.upm.edu.my/

Exploring Venom-derived Peptides from *Calloselasma rhodostoma* Snake as Promising Cholinesterase Inhibitors for Alzheimer's Disease Therapy

Annisa Maghfira[1], Itsar Auliya[1], Tri Rini Nuringtyas[1,2], Fajar Sofyantoro[1], Donan Satria Yudha[1], Slamet Raharjo[3], and Yekti Asih Purwestri[1,2]*

[1]*Department of Tropical Biology, Faculty of Biology, Universitas Gadjah Mada, Yogyakarta 55281, Indonesia*
[2]*Research Center for Biotechnology, Universitas Gadjah Mada, Yogyakarta 55281, Indonesia*
[3]*Department of Internal Medicine, Faculty of Veterinary Medicine, Universitas Gadjah Mada, Yogyakarta 55281, Indonesia*

ABSTRACT

Alzheimer's disease (AD) is a neurodegenerative disorder that primarily affects individuals over 60 years of age, characterized by symptoms such as memory impairment and cognitive decline. The pathogenesis of AD involves multiple factors, including protein misfolding and oxidative stress. A crucial aspect of AD progression is the dysregulation of cholinesterase enzymes, particularly acetylcholinesterase (AChE) and butyrylcholinesterase (BChE), which contribute to neurotoxic amyloid plaques and neurofibrillary tangles. This study investigates the potential of proteins and peptides from the venom of *Calloselasma rhodostoma* as BChE inhibitors, aiming to explore new therapeutic avenues for AD. Venom was extracted, fractionated, and analyzed using ultrafiltration, SDS-PAGE, and LC-HRMS. In vitro assays evaluated the BChE inhibition activity, while in silico molecular docking assessed the binding affinities of the identified peptides. The study identified several venom-derived peptides with significant BChE inhibitory potential, notably CFVVQPWEGK and IDVLSDEPR, which demonstrated strong binding affinities and stability in docking studies. These findings highlight the potential of peptides derived from *C. rhodostoma* venom as natural BChE inhibitors, offering a promising basis for developing novel AD therapies. Further research is warranted to fully understand the mechanisms and therapeutic potential of these bioactive compounds.

Keywords: Alzheimer's disease, butyrylcholinesterase, molecular docking, snake venom, therapeutic peptides

ARTICLE INFO

Article history:
Received: 11 March 2025
Accepted: 10 November 2025
Published: 25 November 2025

DOI: https://doi.org/10.47836/pjtas.48.6.21

E-mail addresses:
annisamaghfira@mail.ugm.ac.id (Annisa Maghfira)
itsarauliya@mail.ugm.ac.id (Itsar Auliya)
tririni@ugm.ac.id (Tri Rini Nuringtyas)
fajar.sofyantoro@ugm.ac.id (Fajar Sofyantoro)
donan.satria@ugm.ac.id (Donan Satria Yudha)
priesta_raharjo@ugm.ac.id (Slamet Raharjo)
yekti@ugm.ac.id (Yekti Asih Purwestri)
* Corresponding author

e-ISSN: 2231-8542

INTRODUCTION

Alzheimer's disease (AD) represents a prevalent neurodegenerative disorder predominantly afflicting individuals aged 60 years and above (Abubakar et al., 2022; Breijyeh & Karaman, 2020; Monteiro et al., 2023; Panachamnong et al., 2014). Various lifestyle factors, such as smoking, alcohol consumption, high cholesterol, and high sugar intake, along with genetic predispositions, exert notable influences on AD susceptibility (P. Chen et al., 2023; Stern et al., 2022). Dementia, an outcome of AD, presents a range of symptoms, including temporal and spatial disorientation, memory impairment, mood swings, and aphasic manifestations (Duce et al., 2019; Liao et al., 2022; van der Schaar et al., 2022). The pathogenesis of AD encompasses protein misfolding, aggregation phenomena, oxidative stress, mitochondrial dysfunction, and neuronal inflammation within cerebral tissues (Bendjedid et al., 2020; Bhushan et al., 2018; Monteiro et al., 2023). Recent pharmacological studies have emphasized the importance of cholinesterase inhibition as a therapeutic strategy for AD management, with heterocyclic scaffolds and flavonoid derivatives being particularly promising (Mughal et al., 2021; Obaid, Mughal, et al., 2022; Obaid, Naeem, et al., 2022).

Central to neurotransmission, acetylcholine (ACh) orchestrates pivotal roles by interacting with cholinesterase enzymes, comprising predominantly acetylcholinesterase (AChE), and to a lesser extent, butyrylcholinesterase (BChE) (Darvesh, 2016; Greig et al., 2005; Makin, 2018; Xing et al., 2021). In physiological states, AChE predominantly facilitates ACh hydrolysis, accounting for approximately 80%, while BChE contributes to roughly 10% (R. Chen et al., 2023; Pereira et al., 2022). Conversely, in AD pathology, elevated AChE activity may lead to amyloid accumulation and neurofibrillary tangle (NFT) formation (Ferreira-Vieira et al., 2016; Ma et al., 2022), potentially diminishing ACh levels (Abubakar et al., 2022; Bhushan et al., 2018). Concurrently, escalated BChE activity may foster neuritic plaque and NFT formation, culminating in cerebral tissue degeneration and clinical dementia manifestations (Liao et al., 2022; Mushtaq et al., 2014; Stern et al., 2022). Furthermore, heightened AChE activity may trigger an escalation in ACh levels, thereby augmenting the activity of BChE in the brain (Darvesh, 2016; Mushtaq et al., 2014). This surge in activity fosters the formation of neocortical amyloid-rich neurotic plaques and NFT, thereby instigating cerebral tissue degeneration and consequent clinical manifestations of dementia (Mushtaq et al., 2014). The dual role of AChE and BChE in both neurotransmission and amyloid aggregation has been further supported by in vitro and in vivo studies of novel cholinesterase inhibitors, including chalcone derivatives and other small molecules that show neuroprotective potential (Al-ghulikah et al., 2023). Importantly, in advanced stages of AD, AChE activity diminishes while BChE activity remains stable or even increases, shifting the regulation of acetylcholine primarily to BChE (Lee et al., 2018; Wright et al., 1993). This highlights the therapeutic relevance of targeting BChE, particularly since most current treatments such as Donepezil are highly AChE-selective, with only Rivastigmine acting as a dual inhibitor (Kandiah et al., 2017; Nordberg et al., 2009).

Snake venom serves not only as a defensive mechanism but also fulfils a pivotal role in prey immobilization (Aird et al., 2015; Fry et al., 2006; Lai & Lu, 2023). Consequently, venom constituents predominantly comprise bioactive agents, encompassing a spectrum of compounds such as carbohydrates, biogenic amines, lipids, purine nucleosides, peptides, and proteins, constituting 70-90% of its composition (Adukauskienė et al., 2011; Chan et al., 2016; Lai & Lu, 2023; Oliveira et al., 2022). The heterogeneity in venom composition is notably influenced by factors such as habitat, seasonal variations, age, gender, and dietary preferences (Durban et al., 2017; Ferreira De Oliveira et al., 2022; Neumann et al., 2020). Interestingly, snake venoms themselves have been screened for intrinsic cholinesterase-inhibiting components, highlighting their potential as natural sources of enzyme inhibitors relevant to AD research (Liesener et al., 2007). *Calloselasma rhodostoma*, commonly known as the Malayan Pit Viper, thrives in tropical climates and prevalent across Southeast Asian territories including Vietnam, Thailand, Malaysia, and the Indonesian archipelago, particularly Borneo and Java Island (Aphrodita et al., 2025; Oh et al., 2021; Tan et al., 2022; Tang et al., 2019). As a constituent of the Viperidae family, which boasts the largest venom gland and longest fangs among its serpentine counterparts, *C. rhodostoma* venom holds considerable intrigue for its potential therapeutic applications (Cerda et al., 2022; Khimmaktong et al., 2022; Kusuma et al., 2023; Tang et al., 2019). In recent years, there has been an increasing focus on researching peptides and proteins as promising candidates for new therapeutic interventions (Chan et al., 2016; Oliveira et al., 2022; Sofyantoro et al., 2022). Several studies have been conducted to identify anticholinesterase activity from snake venom, specifically for the AChE inhibitor. Snake venom proteins that have already been identified as AChE inhibitors are fasciculin-1 and fasciculin-2, which are isolated from green mamba *Dendroaspis angusticeps*. Research has also found that there is AChE inhibition activity in *Bothrops moojeni* venom using ESI/MS and Ellman assay (Karlsson et al., 1984; Liesener et al., 2007). However, the potential of snake venom as a BChE inhibitor is a promising area yet to be explored and needs further investigation. The current study aimed to identify the proteinaceous constituents within *C. rhodostoma* venom and assess their viability as inhibitors of BchE, particularly in the context of Alzheimer's disease.

MATERIALS AND METHODS

Venom Collection

The study protocol was approved by the Ethics Committee of Research and Testing Laboratory (LPPT), Universitas Gadjah Mada, Indonesia (Certificate Number: 00051/04/LPPT/X/2023). Venoms were sourced from *C. rhodostoma*, a member of the Viperidae family from Kaliurang, Yogyakarta, Indonesia. This specimen, encompassing one adult female, was approximately 1 to 2.5 years old. Venom extraction procedures were carried out after a 2-week period of fasting to ensure repletion of the venom glands. The harvested venom was kept at -80°C for 24 hours, followed by freeze-drying to preserve the protein integrity. Upon completion, the powdered venom specimen was stored at -20°C.

Ultrafiltration

Snake venom proteins were separated using Ultrafiltration Vivaspin® Maeso (50, 30, and 10 kDa) and Amicon® Ultrafiltration (3 kDa). Each apparatus underwent a preliminary washing procedure with PBS (0.01 M; pH 7) followed by centrifugation. Five milligrams of venom were dissolved in 2 mL of PBS (0.01M; pH7), followed by centrifugation (5000 rpm; 5 minutes; 4°C). Supernatant was then transferred to the Vivaspin device (50 kDa) and subjected to centrifugation (10,000 rpm; 5 minutes; 4°C). The filtered samples were further refined through successive filtration steps using decreasing filter sizes (50 - 10 kDa). The residual content was obtained through reverse centrifugation (3000 rpm; 3 minutes; 4°C). The filtrate from the 10 kDa filtration stage was subsequently transferred to the Amicon device (3 kDa) and subjected to centrifugation (14,000 G; 30 minutes; 4°C). The resulting residue was obtained through reverse centrifugation (14,000 G; 10 minutes; 4°C). Following these procedures, the fractions, encompassing both filtrates and residues, were preserved at -20°C until subsequent analysis.

Anion Exchange Chromatography

Snake venom protein was subjected to fractionation using a HiTrap Q HP Column (5 mL) as in Tang et al., (2016). Approximately 5 mg of *C. rhodostoma* venom was dissolved in 2 mL of PBS (0.01 M, pH 7) and subsequently subjected to centrifugation at 10,000 rpm for 5 minutes. The supernatant was carefully isolated and subjected to fractionation. The column was initially pre-equilibrated with a starting buffer (Tris HCl 0.02 M, pH 8) followed by elution with NaCl 0.5 M in Tris HCl 0.02 M, pH 8, at a flow rate of 1 mL/min. Fractions were collected at 3 mL intervals over 15 cycles and subsequently stored at -20°C for subsequent analysis.

Protein Quantification

Protein quantification was performed using the Bradford Assay method with Bovine Serum Albumin (BSA) stock solution (1 mg/mL) serving as the standard reference. Samples of 5 µL were combined with 795 µL of distilled water and 200 µL of Bradford reagent. The absorbance was then measured at 595 nm wavelength employing a Spectrophotometer.

SDS-PAGE

In SDS-PAGE analysis, aliquots of 25 µL samples were dispensed into sterile microtubes, followed by the addition of 6.25 µL of 5x sample buffer (Abbkine). Subsequently, the tubes were homogenized using a vortex and sealed with parafilm. These samples underwent incubation at 100°C for 2 - 3 minutes using a water bath, followed by immediate transfer to ice for 15 - 30 minutes, thus undergoing a heat shock treatment. The SDS gel (Q-PAGE TGN Precast Gel; QP4510; SMOBio Technology) was set up within the SDS chamber containing the running buffer. Gel electrophoresis ensued at 80 V for 90 minutes. Post-electrophoresis, the gel was stained utilizing Coomassie Brilliant Blue (CBB) on a shaker overnight. Subsequent destaining involved immersion in a solution comprising 50% methanol, 40% distilled water, and 10% glacial acetic acid on a shaker for 2-3 hours. Upon complete destaining, immersion in 10% glacial acetic acid followed.

Protein Digestion

For protein digestion, a 1 mg venom sample was diluted in 200 µL of MilliQ water as in Tang et al., (2016). From this dilution, 30 µL was aliquoted into a fresh microtube. To this, 4 µL of Protease Max and 2 µL of DTT were added. The mixture underwent incubation at 55°C for 20 minutes within a water bath. Subsequent to this, 2 µL of iodoacetamide was introduced, followed by incubation at room temperature for 15 minutes in the dark. Tris-HCl (100 mM), in a volume three times that of the total mixture, was added, followed by 2 µL of Trypsin Gold (Trypsin Gold, Mass Spectrometry Grade; V5280; Promega). The sample was subjected to overnight incubation at room temperature or incubated at 37°C for 3 hours. The digested protein was subjected to Liquid Chromatography High-Resolution Mass Spectrometry (LC-HRMS) analysis and BChE inhibition assay.

LC-HRMS

Trypsin-digested crude venom and AEC fractions were subjected to LC-HRMS. LC-HRMS analysis was conducted at the Laboratory for Integrated Research and Testing (LPPT), Universitas Gadjah Mada, Indonesia. Samples were injected into the LC-HRMS system, which featured a reverse-phase separation column connected to an EASY-Spray column system (Thermo Scientific Q Exactive benchtop LC-HRMS with High-Performance Quadrupole Precursor and High-Resolution Accurate Mass Orbitrap Detection). Elution was conducted using two mobile phases: mobile phase A (0.1% formic acid in water) and mobile phase B (0.1% formic acid in acetonitrile), with a gradient applied at a flow rate of 100 µL/minute. For mass spectrometry detection, high-resolution and accurate mass mode in positive ion mode were utilized. Subsequently, data from LC-HRMS underwent processing utilizing Proteome Discoverer 3.0 software on a computer system to obtain peptide sequences present in the digested venom, alongside information regarding the master protein, isoelectric point (pI) values, and molecular weight. For data validation, a precursor mass error tolerance of ±10 ppm and a fragment mass error tolerance of ±0.02 Da were applied. Protein identifications were filtered using a false discovery rate (FDR) of <1% at both peptide and protein levels, and only proteins with at least two unique peptides were considered confidently identified.

Inhibition Assay

The evaluation of Butyrylcholinesterase (BChE) inhibition activity was carried out using the Butyrylcholinesterase Inhibitor Screening Kit (Colorimetric; ABCAM) (Li et al., 2021; Obaid, Naeem, et al., 2022). Trypsin-digested crude venom was diluted with 0.3% DMSO. Subsequently, 1 µL of the diluted samples and 9 µL of BChE Assay buffer were dispensed into designated wells, to achieve final concentrations of 200 and 300 ppm. The enzyme control and background control wells received 10 µL of BChE Assay buffer, whereas the positive control well was loaded with 5 µL of Rivastigmine at final concentrations of 200 and 300 ppm. The negative control well was filled with 10 µL of 0.3% DMSO. Each well, excluding the background control well, was supplemented with 5 µL of BChE enzymes. The final volume in each well was adjusted to 80 µL, followed by an incubation period of 30 minutes at room temperature in the absence of light. Subsequently, 20 µL of reaction mix (10 µL of diluted BChE substrate, 5 µL of probe mix, and 5 µL of BChE assay buffer) was loaded into each well. Absorbance readings were recorded using a Microplate Reader at a wavelength of 412 nm, with measurements taken at 5-minute intervals over a total duration of 60 minutes.

Molecular Docking

Molecular docking is an effective method for predicting and aligning target binding sites, exploring potential conformations of compounds, and elucidating the interactions between a ligand and its receptor (Frimayanti et al., 2021; Hidayatullah et al., 2020). Post-acquisition of peptide sequences via LC-HRMS, a meticulous selection process ensued employing ProtParam, ToxinPred, and AllerTop algorithms to discern stable, non-toxic, and non-allergenic peptides. Three-dimensional structure of peptides were modelled using the PEPFOLD4 webserver (https://mobyle2.rpbs.univ-paris-diderot.fr/cgi-bin/portal.py#forms::PEP-FOLD4). Rivastigmine (CID 77991), as a positive control, was obtained through PubChem. BChE receptors were retrieved from Uniprot (Code: P06276) and then modelled using the Swiss Model Expasy web server. As the BChE receptor structure obtained from UniProt does not include a native ligand, Rivastigmine, a clinically established BChE inhibitor, was used as a positive control and benchmark for validating peptide interactions. Ligand and receptor preparation were meticulously executed employing Biovia Discovery, Chimera, and PyMol, followed by molecular docking using

PyRx. The result of protein-peptide docked complexes was rendered visually utilizing PyMol and Discovery Studio.

ADMET Prediction

The Simplified Molecular Input Line Entry System (SMILES) structural format of the two best peptides from the molecular docking result was acquired using a web-based tool, PepSMI (https://www.novoprolabs.com/tools/convert-peptide-to-smiles-string). The PepSMI web server will convert the peptide sequences into SMILES. The ADMET evaluation was carried out using ADMETlab 3.0 web server (https://admetlab3.scbdd.com/) by entering the peptide's SMILES (Xiong et al., 2021). Then, Absorption, Distribution, Metabolism, Excretion, and Toxicity properties, including several parameters such as Human Intestinal Absorption (HIA), Papp/Caco-2 permeability, Blood-Brain Barrier (BBB), Plasma Protein Binding (PPB), CYP1A2 inhibitor-substrate, CYP3A4 inhibitor-substrate, T½ Half-Life, hERG blockers, Drug Induced Liver Injury (DILI), Ames mutagenicity, and Human Hepatoxicity were examined using the ADMETlab 3.0 webserver.

RESULTS AND DISCUSSION

SDS-PAGE Analysis

The initial determination of the protein concentration within the crude venom revealed a concentration of 40 µg/mL. Subsequent ultrafiltration procedures were conducted, segregating the filtrate and residue across varying molecular weight cut-off (MWCO) filters (50, 30, 10, and 3 kDa). Notably, the protein concentration within the residues surpassed that of the filtrates. Specifically, the residue obtained from the 50 kDa filter exhibited a protein concentration of 13.60 µg/mL, in stark contrast to the filtrate's concentration of 5.70 µg/mL. Similarly, the filtrates from the 30 kDa and 10 kDa filters displayed protein concentrations of 7.02 µg/mL and 8.53 µg/mL, respectively. Notably, no residue was obtained from the filtrates of these two filter sizes. Conversely, the residue from the 3 kDa filter demonstrated a protein concentration of 44.38 µg/mL, while its filtrate showcased a concentration of 11.21 µg/mL. These quantifications underscored the presence of a protein-enriched fraction resulting from Anion Exchange Chromatography (AEC), with the highest observed protein concentration within one of the 15 fractions derived from the venom of *C. rhodostoma*, amounting to 11.02 µg/mL.

Figure 1A shows 11 discernible protein bands evident within the SDS gel. These identified molecules within the crude venom spanned molecular weights ranging from approximately 13.68 to 115.08 kDa. This observation highlighted distinct protein clusters visualized within the SDS gel, indicative of disparate molecular size ranges. SDS-PAGE analysis of proteins harvested from AEC revealed 9 distinct bands within the fraction derived from *C. rhodostoma* snake venom (Figure 1B), spanning molecular weights from 14.74 to 67.49 kDa. Figure 1B illustrates that the bands observed in the residue on the SDS gel are frequently characterized by smearing. This phenomenon is attributed to the filtration process, as outlined in the device manual, wherein residue concentration typically occurs during centrifugation, consequently resulting in smearing during SDS-PAGE analysis.

Notably, discrepancies in protein banding patterns were discernible among the filtrates from each filtration step. Particularly, filtrates from filters with smaller MWCO exhibited fewer discernible bands in comparison to those from larger filters (Figure 1C). Commencing with the 50 kDa residue (R50) displaying 12 bands, the subsequent filtrate (F50) exhibited a reduced band count of approximately 5. A further decline in band count was evident in the subsequent filtrate of 30 kDa (F30), manifesting only 2 bands. These banding patterns persisted in subsequent filtrates, namely filtrate 10 kDa (F10) and filtrate 3 kDa (F3).

Snake venom, traditionally perceived as predominantly proteinaceous with concentrations ranging between 70% to 90%, exhibits variability across different snake families (Fry et al., 2006; Oliveira et al., 2022; Vejayan et al., 2010). Protein content in the Colubridae family was found to range from 49.8% to 96.4% (Hill & Mackessy, 1997). Factors such as freeze-drying and improper storage conditions can influence protein concentration, potentially leading to sample degradation (Sofyantoro et al., 2024; Vejayan et al., 2010).

The SDS-PAGE analysis of the protein content in the crude venom and its subsequent fractions reveals a complex and heterogeneous protein composition. The differential

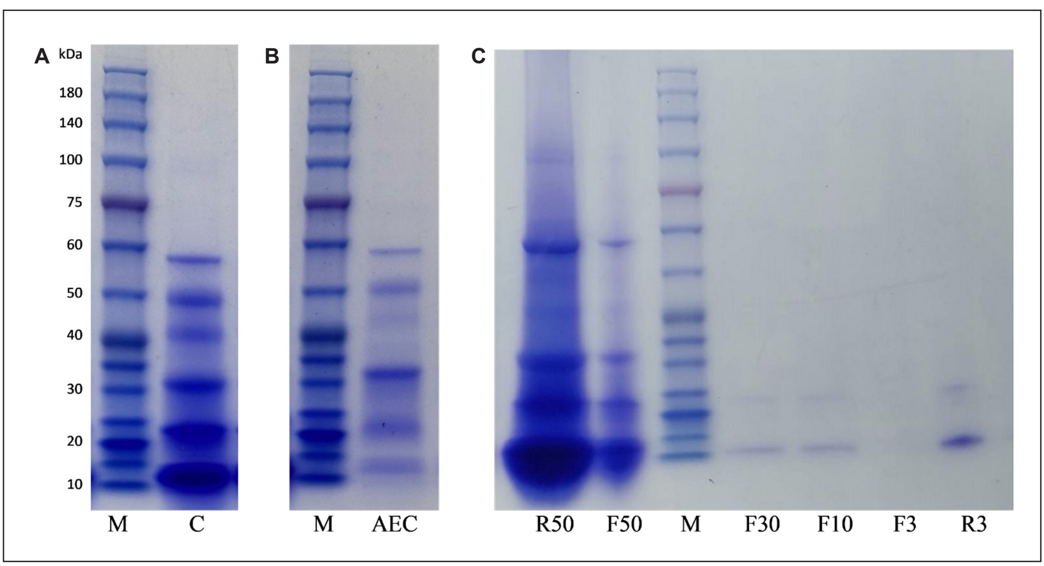

Figure 1. Electrophoretic analysis via SDS-PAGE depicting (A) crude venom, (B) Anion Exchange Chromatography (AEC) fractions, and (C) ultrafiltration fractions of *C. rhodostoma* snake venom. M: marker; C: crude venom; AEC: Anion Exchange Chromatography fractions; R50: 50 kDa residue; F50: 50 kDa filtrate; M: marker; F30: 30 kDa filtrate; F10: 10 kDa filtrate; F3: 3 kDa filtrate; R3: 3 kDa residue

protein concentrations observed across various molecular weight cut-off (MWCO) filters underscore the selective retention and passage of proteins based on size. The stark contrast in protein concentrations between residues and filtrates, especially in the 50 kDa and 3 kDa filters, indicates that larger proteins are predominantly retained, while smaller proteins pass through. The presence of multiple distinct protein bands, ranging from 13.68 to 115.08 kDa in the crude venom, highlights the diversity of protein sizes. The progressive reduction in the number of protein bands in the filtrates as the MWCO decreases suggests effective size-based separation. However, the smearing of protein bands, particularly in the residues, likely results from the concentration process during filtration, as noted in the device manual. This phenomenon could indicate potential aggregation or degradation during processing, warranting further optimization of the filtration protocol. Moreover, the identification of nine distinct bands in the fraction derived from anion exchange chromatography, spanning molecular weights from 14.78 to 67.49 kDa, suggests a selective enrichment of specific protein subsets. These findings provide a foundational understanding of the protein composition and separation dynamics in *C. rhodostoma* venom, offering valuable insights for future studies on the functional and toxicological properties of these proteins.

In vitro Inhibition Activity of BChE

The observed in vitro inhibition activities unveiled that the trypsin-digested crude venom of *C. rhodostoma*, administered at a concentration of 200 ppm, showed an estimated BChE inhibition of 43.75% (Table 1). Similarly, at a concentration of 300 ppm, the trypsin-digested venom exhibited an inhibition activity of 25%. In contrast, compared to the positive control (Rivastigmine), concentrations of 200 ppm displayed inhibition activity of 91.67%, while concentrations of 300 ppm showed inhibition activity of 93.75% (Table 1).

The observed inhibition activity of BChE by the trypsin-digested crude venom of *C. rhodostoma* demonstrates a dose-dependent response, with higher concentrations (300 ppm) not consistently leading to increased inhibition compared to lower concentrations (200 ppm). This suggests the presence of both inhibitory and potentially counteractive components within the trypsin-digested venom. The variation in inhibition percentages, ranging from 25% to 43.75%, indicates a complex interaction between the venom

Table 1
Evaluation of the inhibitory efficacy of trypsin-digested crude venom against Butyrylcholinesterase (BChE)

Samples	Concentration (ppm)	Inhibition Activity (%)
Trypsin-digested crude venom	200	43.75
	300	25
Rivastigmine	200	91.67
	300	93.75

constituents and BChE. In contrast, the positive control, Rivastigmine, exhibited significantly higher inhibition rates (91.67% to 93.75%), underscoring its potency and specificity as a BChE inhibitor. The lower efficacy of the venom might be attributed to the crude nature of the extract, which could contain a mixture of compounds with varying levels of inhibitory activity. These findings highlight the need for further fractionation and identification of active components within the venom to elucidate the specific mechanisms underlying BChE inhibition. Additionally, comparing these results with those from other snake venoms or natural sources could provide insights into unique or shared biochemical pathways. Although the observed inhibition percentages were lower than those of the positive control, the significance of these findings lies in the successful identification of novel peptides with measurable BChE inhibitory activity. This preliminary evidence provides an important foundation for future optimization and structural modification aimed at improving potency and therapeutic potential. It should also be noted that only two concentrations were tested in this preliminary screening, which was sufficient to identify promising inhibitory activity but limited in providing detailed dose–response relationships. More comprehensive concentration-dependent assays will be needed in future studies to validate and expand upon these findings.

In silico Inhibition Activity Assessment

Analysis of LC-HRMS from crude venom data revealed the presence of 15 proteins across 5 distinct protein families within the crude venom of *C. rhodostoma* (Supplementary Table 1). These families encompass L-Amino Acid Oxidase, Snake Venom Metalloproteinase Kistomin, Zinc Metalloproteinase or Disintegrin, Snaclec Rhodocytin subunit beta, Snaclec Rhodocentin subunits alpha, beta, delta, and gamma, Thrombin-like Enzyme, Acidic and Basic Phospholipase A2. Moreover, the crude venom exhibited a spectrum of 136 identified peptide sequences upon trypsin digestion (Supplementary Table 2). Conversely, samples isolated through AEC revealed 10 proteins spanning 4 protein families, including Zinc Metalloproteinase or Disintegrin, Snake Venom Metalloproteinase Kistomin, Thrombin-like Enzyme Ancrod, Snaclec Rhodocentin subunits alpha, beta, delta, and gamma, Snaclec Rhodocytin subunit alpha, and Basic Phospholipase A2 (Supplementary Table 3). Meanwhile, a total of 42 peptide sequences were discerned from the trypsin-digested venom subjected to Anion Exchange Chromatography (Supplementary Table 4).

Peptide sequences were chosen based on their physicochemical attributes, including stability, non-toxicity, and non-allergenicity. This selection process yielded 12 peptide sequences from the crude venom (Table 2) and 7 peptide sequences from AEC (Table 3). All identified peptide sequences underwent docking simulations using PyRx to assess their inherent inhibitory activity against BChE. The docking outcomes revealed diverse binding modes, characterized by varying binding affinities and RMSD values. Modes

Table 2
Evaluation of binding affinity and RMSD values for peptide components derived from trypsin digestion of C. rhodostoma crude venom against BChE

No.	Peptide Sequence	Mode	Binding Affinity (kcal/mol)	RMSD (Å)
	Rivastigmine (control)	3	-6.3	0.965
1.	NEEAGWYANLGPMR	2	-7.9	2.834
2.	DCADIVFNDLSLIHQLPK	2	-6.5	2.651
		6	-6.2	2.67
3.	DFDGNTVGLAFVGGICNEK	3	-6.3	2.231
		8	-6.1	3.203
4.	YCAGVVQDHTK	1	-7.6	2.36
		3	-7.5	2.055
		8	-6.9	2.773
5.	LEAVFVDMVMENNFENK	1	-7	1.541
6.	SNLEWSDGSSISYENLYEPYMEK	3	-6.4	2.891
		8	-6	2.525
7.	GPNPCAQPNKPALYTSIYDYR	2	-7	2.251
		4	-6.9	1.93
8.	DELADEDYVWIGLR	1	-7	1.674
9.	EQQCSSEWSDGSSVSYENLIDLHTK	1	-6.3	2.021
		4	-5.7	2.024
10.	CFVVQPWEGK	2	-7.8	2.226
11.	QAENGHLVSIGSAAEADFLDLVIVVNFDK	8	-4.7	2.042
12.	GHLVSIGSDGEADFVAQLVTNNIK	2	-7.2	2.516
		4	-7.1	2.187
		6	-7.1	2.114

meeting predefined criteria for both binding affinity and RMSD were deemed indicative of peptides' potential to inhibit BChE activity (Table 2 and Table 3).

Table 2 demonstrates the binding affinities of peptides derived from crude venom, ranging from -4.7 to -7.9 kcal/mol, while Table 3 showcases the binding affinities of peptides from AEC samples, ranging from -6.5 to -8.8 kcal/mol. A more negative binding affinity indicates a stronger interaction between the peptide and the BChE receptor (Alsedfy et al., 2024). Notably, within Table 2, the sequence CFVVQPWEGK (mode 2) exhibits the highest affinity value of -7.8 Å and a favorable RMSD value of 2.226 kcal/mol among peptides from crude venom. Conversely, from Table 3, the peptides from AEC samples highlight the sequence IDVLSDEPR (mode 2) with the highest affinity value of -8.8 Å and a commendable RMSD value of 2.228 kcal/mol. Considering the binding affinity and RMSD scores of CFVVQPWEGK and IDVLSDEPR, it can be inferred that these two sequences demonstrate the most promising interaction with the BChE receptor.

The 3D visualization of the interaction between the CFVVQPWEGK peptide and the BChE receptor is depicted in Figure 2A. Similarly, the interaction between the IDVLSDEPR peptide and the BChE receptor is illustrated in Figure 2B. As illustrated in Figure 3A, CFVVQPWEGK binds with BChE with amino acid residues Trp110, Asp98, Leu314, Gly361, Phe306, Pro309, Tyr310, Gln95, Leu301, Ala305, Asn96, Pro387, Thr312 and Phe357 engage in van der Waals interactions (Figure 3A). Meanwhile, as illustrated in Figure 3B, the active peptide ligand IDVLSDEPR binds with Ser107, Asp98, Ala356, Asn111, Gly149, His466, Gly467, Tyr468, Gly145, Val316, Leu314, Ser315, Gln95, Glu304, Thr312, Gln147, and Gly361 of receptor amino acid residues through van der Waals interactions. A comprehensive depiction of the interactions occurring between the ligand and the amino acid residues within the BChE receptor is provided in Table 4.

Table 3
Binding affinity and Root Mean Square Deviation (RMSD) analysis of peptides derived from trypsin-digested Anion Exchange Chromatography fractions of C. rhodostoma *venom against BChE*

No.	Peptide Sequence	Mode	Binding Affinity (kcal/mol)	RMSD (Å)
1.	IDVLSDEPR	2	-8.8	2.228
		4	-8.7	2.291
		6	-8.6	2.297
		7	-8.6	2.871
2.	VLCAGDLR	1	-7.5	2.618
		2	-7.5	1.857
		3	-7.3	2.182
		4	-7.1	2.418
		5	-7.1	2.307
		6	-7	3.177
		8	-7	2.725
3.	SWIGLK	1	-8.7	2.052
		2	-8.5	1.896
4.	CFVVQPWEGK	2	-8.8	2.381
		3	-8.8	2.257
		4	-8.5	2.61
5.	DFDGNTVGLAFVGGICNEK	1	-6.8	1.367
		4	-6.7	1.887
		8	-6.5	2.807
6.	LASQTLK	1	-7.5	2.496
		2	-7.3	2.903
		3	-7.2	2.781
		7	-7	2.195
7.	DELADEDYVWIGLR	2	-7.7	1.942
		4	-7.5	2.244

Table 4
Computational analysis of molecular interactions between peptides derived from trypsin digestion of C. rhodostoma *venom and the BChE receptor using the PyRx application*

Ligand	Carbon Hydrogen Bond	Conventional Hydrogen Bond	Van Der Waals	Other Types of Bond Formation
Rivastigmine (Control)	Tyr468 Gly106	-	Ser107 His466 Asp98 Thr148 Gly144 Gly467	Pi-Pi Stacked Trp110 Pi Alkyl / Alkyl Tyr360 Ala356 Trp458
CFVVQPWEGK	Pro313 Gly311	Gly311 Ile384 Val308 Asn317 Gln147 Glu304	Phe357 Gly145 Leu314 Asn111 Asp98 Trp110 Thr312 Pro387 Ala305 Gly361 Phe306 Pro309 Tyr310 Gln95 Leu301 Asn96	Amide-Pi Stacked Gly144 Pi-Alkyl / Alkyl Tyr360
IDVLSDDEPR	Trp110 Ala305 Gly144 Gln147	Pro313 Asn317 Asn96 Gly311	Ser107 Asp98 Ala356 Asn111 Gly149 His466 Gly467 Tyr468 Gly145 Val316 Leu314 Ser315 Gln95 Glu304 Thr312 Gln147 Gly361	Pi-Sigma Tyr360 Pi-Alkyl Phe357 Trp110

Previous research has shown that hydrogen bonds help to improve the binding and AChE inhibitory activity (Lu et al., 2011; Obaid, Mughal, et al., 2022; Obaid, Naeem, et al., 2022; Peitzika & Pontiki, 2023). Hydrogen bonds play an important role to stabilize the ligand inside the catalytic triad. The active peptide ligand CFVVQPWEGK is observed

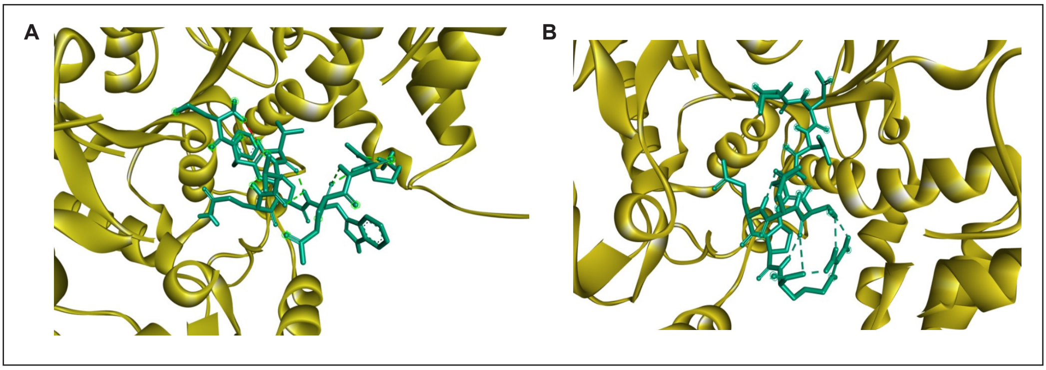

Figure 2. Three-Dimensional visualization illustrating the interactions between (A) CFVVQPWEGK and (B) IDVLSDEPR peptides with the Butyrylcholinesterase (BChE) receptor. Yellow: BChE; green: peptides

binding to Gly311, Ile384, Val308, Asn317, Gln147, and Glu304, as well as IDVLSDEPR binds to Pro313, Asn317, Asn96, and Gly311 in hydrogen bonds. Hydrogen bonds enhance the binding affinity of these peptides. The π-π interactions, hydrogen bonds, and strong hydrophobic interactions between the ligand and AChE inhibit AChE's activity by competing for the acetylcholine binding site. These interactions may also prevent amyloid fibrillogenesis by blocking the beta-amyloid recognition zone at the peripheral site. In recent studies, N-, O-, and S- based heterocyclic agents have demonstrated potential anti-cholinesterase activity. Their easy preparation, low toxicity, and high bioavailability are driving their increasing use (Lu et al., 2011; Obaid, Mughal, et al., 2022; Obaid, Naeem, et al., 2022; Peitzika & Pontiki, 2023).

In human catalytic BChE, the active site of BChE is positioned in a deep gorge with specific amino acid keys such as Ser226, His466, and Glu353 surrounded by six amino acids. At the lip of the active site, the substrate interacts with aspartic acid (Asp) and tyrosine (Tyr). Tryptophan (Trp) facilitates the creation of an anionic site (Jovičić, 2024). Molecular docking analysis shows that the CFVVQPWEGK ligands may not interact with the active site of the BChE enzyme, indicating they likely inhibit the enzyme through other sites. On the other hand, IDVLSDEPR and Rivastigmine interact with the active site of BChE with only one amino acid key residue, His666, with van der Waals interaction.

In the docking analysis of Rivastigmine (Table 2; Figure 4), it is apparent that the ligand engages with the BChE, displaying a binding affinity of -6.3 kcal/mol and an RMSD value of 0.965 Å. Comparative scrutiny between the docking outcomes of Rivastigmine as the reference and the active peptide ligand sequences CFVVQPWEGK and IDVLSDEPR derived from crude venom and AEC showcases concordant specific amino acid residues pivotal in BChE receptor interaction. As delineated in Figure 4 and Table 4, the Rivastigmine ligand forms van der Waals interactions with Thr 148, Asp 98, His 466, Ser 107, Gly 144, and Gly 467.

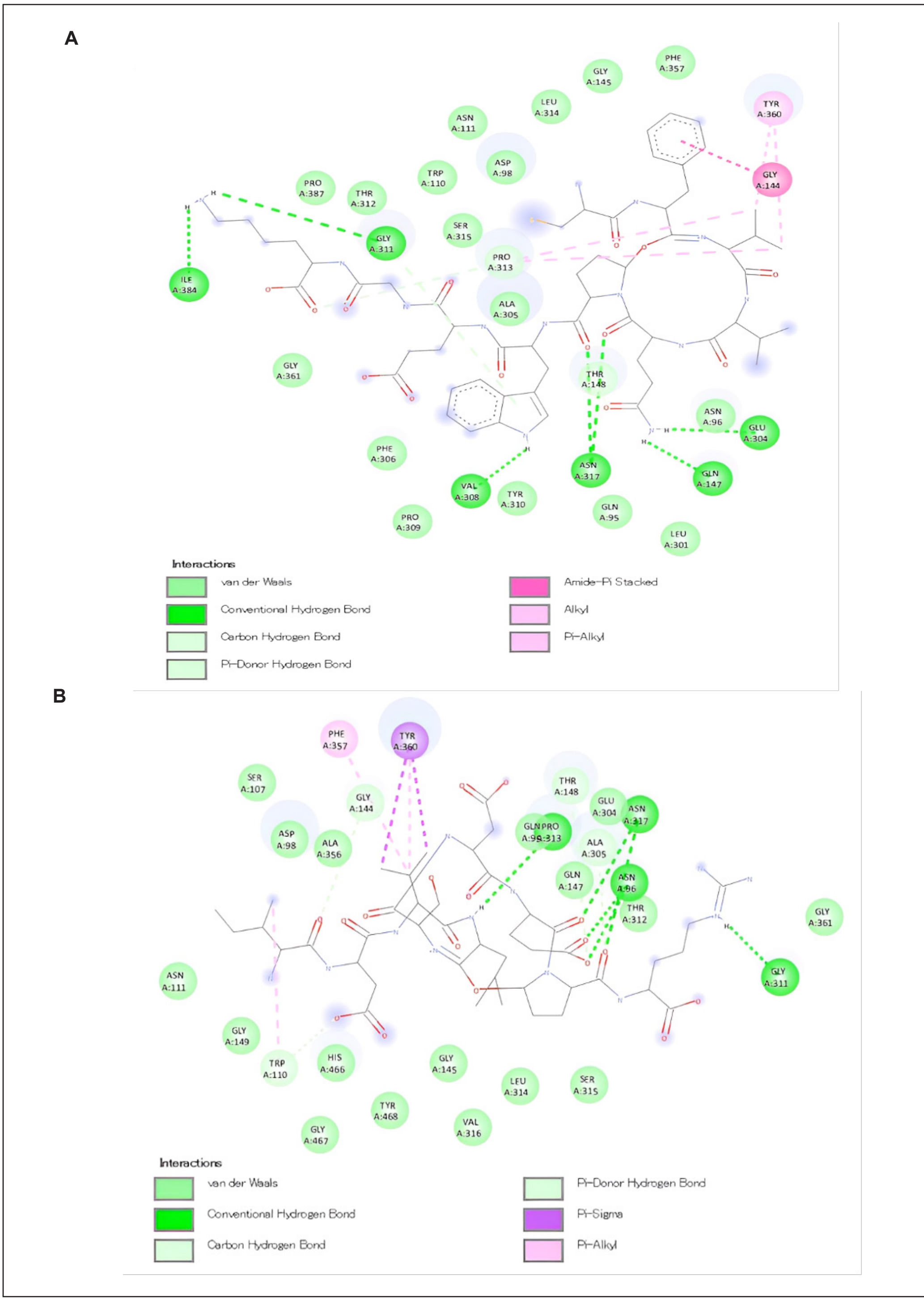

Figure 3. Two-Dimensional visualization of the molecular interaction between (A) CFVVQPWEGK and (B) IDVLSDEPR peptides with the Butyrylcholinesterase (BChE) receptor

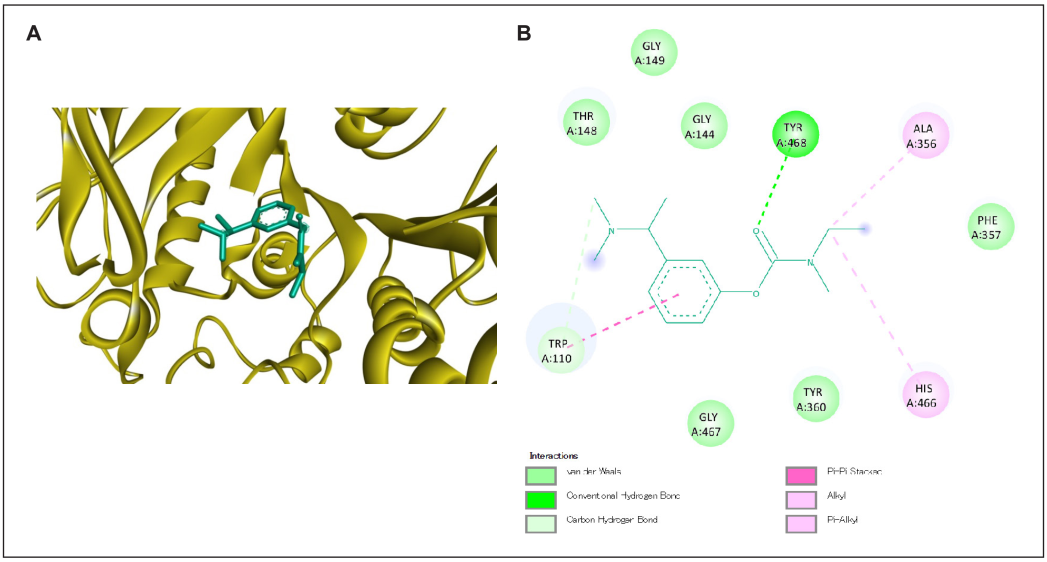

Figure 4. (A) Three-dimensional (3D) and (B) two-dimensional (2D) representations of the molecular interaction between Rivastigmine (control) and the Butyrylcholinesterase (BChE) receptor. Yellow: BChE; green: Rivastigmine

The in-silico inhibition activity assessment of trypsin-digested peptides from the crude venom and AEC samples from *C. rhodostoma* provides a comprehensive view of the venom's biochemical diversity and potential therapeutic applications. The identification of 15 proteins across five distinct families in the crude venom, including L-Amino Acid Oxidase, Snake Venom Metalloproteinases (like Kistomin), Zinc Metalloproteinases or Disintegrins, Snaclec Rhodocytin and Rhodocentin subunits, Thrombin-like Enzymes, and Acidic and Basic Phospholipase A2, underscores the complex nature of snake venoms. The detection of 136 peptide sequences further highlights the intricate peptide landscape within the venom. In contrast, the AEC samples, which revealed 10 proteins spanning four families and 42 peptide sequences, suggest that chromatographic techniques can effectively enrich specific bioactive components, potentially offering a more targeted approach to peptide isolation.

The docking simulations using PyRx revealed significant variations in binding affinities and Root Mean Square Deviation (RMSD) values among the identified peptides, suggesting a range of inhibitory activities against BChE. Notably, peptides such as CFVVQPWEGK and IDVLSDEPR demonstrated the strongest binding affinities, with values reaching -7.8 kcal/mol and -8.8 kcal/mol, respectively. These values indicate a strong interaction with the BChE receptor, surpassing the binding affinity of the control compound, Rivastigmine, which was -6.3 kcal/mol. The detailed molecular interactions, particularly van der Waals interactions and hydrogen bonds with key residues like Trp 110, Asp 98, and Gly 467, highlight the specificity of these peptides in binding to BChE.

The variations in peptide sequences and binding affinities between the crude venom and AEC samples underscore the importance of peptide diversity in modulating enzymatic activity. The results suggest that specific peptides, potentially more concentrated or isolated through AEC, may offer more potent inhibition of BChE. This finding aligns with the broader pharmacological interest in identifying and optimizing venom-derived peptides for therapeutic use, particularly as inhibitors of cholinesterases, which are relevant in the treatment of neurodegenerative diseases like Alzheimer's.

Absorption, Distribution, Metabolism, Excretion, and Toxicity (ADMET) Prediction

The two best peptides identified through virtual screening and molecular docking were analyzed for their ADMET properties. ADMET evaluation was performed to predict pharmacology and pharmacodynamic properties. By assessing the molecule's ADMET scores, drug pharmacokinetics in the human body can be predicted (Flores-Holguín et al., 2021; Sarkar et al., 2021). The result of the ADMET prediction for the lead peptides is presented in Table 5, along with a comparative analysis with Rivastigmine as a positive control. CFVVQPWEGK and IDVLSDEPR exhibit quite similar properties in ADMET evaluation. In the absorption category, human intestinal absorption (HIA) results are positive for all peptides, excluding Rivastigmine, which has a negative HIA, indicating that the absorption of peptides in the intestine is poorly absorbed compared to Rivastigmine. However, the Caco-2 permeability of the two lead peptides is poor compared to Rivastigmine, which exhibits optimal permeability. Drug bioavailability is determined by its absorption in the body after oral administration (Flores-Holguín et al., 2021). The ability of a peptide to traverse the Blood-Brain Barrier (BBB) is assessed through the BBB permeability index. BBB and Central Nervous System (CNS) permeability are important factors in designing an Alzheimer's drug candidate (Abdelazeem et al., 2024). Both CFVVQPWEGK and IDVLSDEPR peptides, as well as Rivastigmine, show BBB-positive results and optimal plasma protein binding (PPB), suggesting they can effectively penetrate the BBB. Regarding metabolism, none of the peptides or Rivastigmine inhibit the CYP1A2 and CYP3A4 enzymes, indicating that these peptides may enhance metabolism (Abdul-Hammed et al., 2021). Similar to Rivastigmine, the peptides CFVVQPWEGK and IDVLSDEPR display a short half-life. In terms of toxicity, several parameters were assessed, including hERG blockers, drug-induced liver injury (DILI), Ames mutagenicity (AMES), and human hepatotoxicity. All lead peptides and Rivastigmine were found to be non-blockers, non-toxic to the liver, and AMES-negative. Nonetheless, the human hepatotoxicity results raised the possibility of toxicity for the two peptides, including Rivastigmine. These findings indicate that the CFVVQPWEGK and IDVLSDEPR peptides from *C. rhodostoma* venom are able to cross the BBB and imply the potential safety as a new drug candidate.

Table 5
The ADMET prediction of the best two peptides along with Rivastigmine as a positive control

Category	Property (unit)	CFVVQPWEGK		IDVLSDEPR		Rivastigmine		Inference/references range
Absorption	HIA/Human Intestinal Absorption (%)	1.000	HIA Positive	1.000	HIA Positive	0.001	HIA Negative	HIA>0.3: HIA Positive, HIA<0.3: HIA Negative; or 0-0.3: excellent; 0.3-0.7: medium; 0.7-1.0: poor
	Papp/Caco-2 permeability (cm/s)	-6.223	Poor	-6.369	Poor	-4.639	Optimal	Optimal: higher than -5.15 Log unit
Distribution	BBB/Blood Brain Barrier Penetration (%)	0.000	BBB Positive	0.000	BBB Positive	0.734	BBB Positive	BBB≥0: BBB Positive, BBB<0.1: BBB Negative
	PPB/Plasma Protein Binding (%)	19.700	Optimal	20.197	Optimal	37.035	Optimal	PPB<90%: Optimal; PPB>90%: Low Therapeutic Index
Metabolism	CYP1A2-Inhibitor	0.000	Non-inhibitor	0.000	Non-inhibitor	0.477	Non-inhibitor	>0.5: An inhibitor; <0.5: Non-inhibitor
	CYP1A2-Substrate	0.000	Non-substrate	0.000	Non-substrate	0.982	Substrate	>0.5: An substrate; <0.5: Non-substrate
	CYP3A4-Inhibitor	0.000	Non-inhibitor	0.000	Non-inhibitor	0.018	Non-inhibitor	>0.5: An inhibitor; <0.5: Non-inhibitor
	CYP3A4-Substrate	0.000	Non-substrate	0.000	Non-substrate	0.965	Substrate	>0.5: An substrate; <0.5: Non-substrate
Excretion	T1/2/Half-life (H)	0.916	Short half-life	1.321	Intermediate short half-life	0.999	Short half-life	Long half-life: >3 h; Short half-life: <3 h
Toxicity	hERG blockers	0.001	Non blocker	0.000	Non blocker	0.319	Non-blocker	>0.5: Blocker; <0.5: Non blocker
	DILI/Drug Induced Liver Injury	0.267	Non-toxic to liver	0.059	Non-toxic to liver	0.312	Non-toxic to liver	>0.5: Toxic to liver; <0.5: Non toxic to liver
	AMES (Ames Mutagenicity)	0.064	Negative	0.004	Negative	0.326	Negative	>0.5: Positve; <0.5: Negative
	Human Hepatoxicity	0.544	Probability of being toxic	0.11	Probability of being toxic	0.797	Probability of being toxic	0-0.3: excellent; 0.3-0.7: medium; 0.7-1.0: poor

Taken together, the differential binding modes observed for these peptides provide valuable insights into the structure-activity relationships that govern their interactions with the BChE receptor. This knowledge is crucial for the rational design of peptide-based inhibitors, where modifications to enhance binding affinity and specificity can be guided by the docking results. The ADMET prediction also indicates that our peptides nearly met the pharmacokinetics criteria for a drug-like molecule. The study's comprehensive approach, combining LC-HRMS analysis, peptide sequencing, and in silico docking, and ADMET evaluation, provides a robust framework for exploring the therapeutic potential of venom-derived peptides. These findings pave the way for future studies focusing on the functional characterization of these peptides and their development as leads in drug discovery. While molecular dynamics (MD) simulations would provide deeper insights into peptide–BChE interactions, this study was limited to docking-based screening as an initial step, and MD analysis is planned for future validation of the most promising candidates.

CONCLUSION

This study successfully isolated and identified specific protein components from the venom of *C. rhodostoma*, revealing their potential as inhibitors of BChE. The venom's protein and peptide fractions demonstrated promising inhibitory activity against BChE, suggesting a possible application in the management of Alzheimer's disease (AD). Notably, two peptides, CFVVQPWEGK and IDVLSDEPR, exhibited the highest binding affinities and optimal interactions with BChE, positioning them as candidates for further investigation. Looking ahead, there is a compelling need for in vivo studies to evaluate the efficacy and safety of these peptides in animal models of AD. Additionally, further refinement of peptide isolation techniques could enhance the purity and yield of these bioactive compounds. Understanding the detailed mechanisms through which these peptides interact with BChE at a molecular level will be crucial for the development of new therapeutic strategies. Exploration of venom components from other snake species may also yield novel inhibitors, broadening the scope of potential treatments. Ultimately, these endeavours could lead to the development of innovative therapeutics for neurodegenerative diseases, offering hope for more effective management options for patients with AD.

ACKNOWLEDGEMENT

We extend our gratitude to Ananto Puradi and Budi Khoiri Ardiansyah for their invaluable assistance and support throughout the course of this study.

REFERENCES

Abdelazeem, N. M., Aboulthana, W. M., Hassan, A. S., Almehizia, A. A., Naglah, A. M., & Alkahtani, H. M. (2024). Synthesis, in silico ADMET prediction analysis, and pharmacological evaluation of sulfonamide derivatives tethered with pyrazole or pyridine as anti-diabetic and anti-Alzheimer's agents. *Saudi Pharmaceutical Journal*, *32*(5), 102025. https://doi.org/10.1016/j.jsps.2024.102025

Abdul-Hammed, M., Adedotun, I. O., Falade, V. A., Adepoju, A. J., Olasupo, S. B., & Akinboade, M. W. (2021). Target-based drug discovery, ADMET profiling and bioactivity studies of antibiotics as potential inhibitors of SARS-CoV-2 main protease (Mpro). *VirusDisease*, *32*(4), 642–656. https://doi.org/10.1007/s13337-021-00717-z

Abubakar, M. B., Sanusi, K. O., Ugusman, A., Mohamed, W., Kamal, H., Ibrahim, N. H., Khoo, C. S., & Kumar, J. (2022). Alzheimer's Disease: An Update and Insights Into Pathophysiology. *Frontiers in Aging Neuroscience*, *14*, 742408. https://doi.org/10.3389/fnagi.2022.742408

Adukauskienė, D., Varanauskienė, E., & Adukauskaitė, A. (2011). Venomous Snakebites. *Medicina*, *47*(8), 461. https://doi.org/10.3390/medicina47080061

Aird, S. D., Aggarwal, S., Villar-Briones, A., Tin, M. M.-Y., Terada, K., & Mikheyev, A. S. (2015). Snake venoms are integrated systems, but abundant venom proteins evolve more rapidly. *BMC Genomics*, *16*(1), 647. https://doi.org/10.1186/s12864-015-1832-6

Al-ghulikah, H. A., Mughal, E. U., Elkaeed, E. B., Naeem, N., Nazir, Y., Alzahrani, A. Y. A., Sadiq, A., & Shah, S. W. A. (2023). Discovery of chalcone derivatives as potential α-glucosidase and cholinesterase inhibitors: Effect of hyperglycemia in paving a path to dementia. *Journal of Molecular Structure*, *1275*, 134658. https://doi.org/10.1016/j.molstruc.2022.134658

Alsedfy, M. Y., Ebnalwaled, A. A., Moustafa, M., & Said, A. H. (2024). Investigating the binding affinity, molecular dynamics, and ADMET properties of curcumin-IONPs as a mucoadhesive bioavailable oral treatment for iron deficiency anemia. *Scientific Reports*, *14*(1), 22027. https://doi.org/10.1038/s41598-024-72577-8

Aphrodita, A., Sentono, D. N., Yudha, D. S., Purwestri, Y. A., Nuringtyas, T. R., Raharjo, S., Wahid, I., Rahmi, S. N., Wahyudi, S. T., & Sofyantoro, F. (2025). Comparative analysis of hemotoxic, myotoxic, and inflammatory profiles of Calloselasma rhodostoma and Trimeresurus insularis venoms in mice. *Narra J*, *5*(2), 1–16.

Bendjedid, S., Djelloul, R., Tadjine, A., Bensouici, C., & Boukhari, A. (2020). In vitro assessment of total bioactive contents, antioxidant, anti-alzheimer and antidiabetic activities of leaves extracts and fractions of Aloe vera. *Natural and Life Sciences Communications*, *19*(3), 469–485.

Bhushan, I., Kour, M., Kour, G., Gupta, S., Sharma, S., & Yadav, A. (2018). Alzheimer's disease: Causes & treatment – A review. *Annals of Biotechnology*, *1*(1). https://doi.org/10.33582/2637-4927/1002

Breijyeh, Z., & Karaman, R. (2020). Comprehensive Review on Alzheimer's Disease: Causes and Treatment. *Molecules (Basel, Switzerland)*, *25*(24), 5789. https://doi.org/10.3390/molecules25245789

Cerda, P. A., Crowe-Riddell, J. M., Gonçalves, D. J. P., Larson, D. A., Duda, T. F., & Davis Rabosky, A. R. (2022). Divergent Specialization of Simple Venom Gene Profiles among Rear-Fanged Snake Genera (Helicops and Leptodeira, Dipsadinae, Colubridae). *Toxins*, *14*(7), 489. https://doi.org/10.3390/toxins14070489

Chan, Y. S., Cheung, R. C. F., Xia, L., Wong, J. H., Ng, T. B., & Chan, W. Y. (2016). Snake venom toxins: Toxicity and medicinal applications. *Applied Microbiology and Biotechnology*, *100*(14), 6165–6181. https://doi.org/10.1007/s00253-016-7610-9

Chen, P., Yao, H., Tijms, B. M., Wang, P., Wang, D., Song, C., Yang, H., Zhang, Z., Zhao, K., Qu, Y., Kang, X., Du, K., Fan, L., Han, T., Yu, C., Zhang, X., Jiang, T., Zhou, Y., Lu, J., … Liu, Y. (2023). Four Distinct Subtypes of Alzheimer's Disease Based on Resting-State Connectivity Biomarkers. *Biological Psychiatry*, *93*(9), 759–769. https://doi.org/10.1016/j.biopsych.2022.06.019

Chen, R., Li, X., Chen, H., Wang, K., Xue, T., Mi, J., Ban, Y., Zhu, G., Zhou, Y., Dong, W., Tang, L., & Sang, Z. (2023). Development of the "hidden" multi-target-directed ligands by AChE/BuChE for the treatment of Alzheimer's disease. *European Journal of Medicinal Chemistry*, *251*, 115253. https://doi.org/10.1016/j.ejmech.2023.115253

Darvesh, S. (2016). Butyrylcholinesterase as a Diagnostic and Therapeutic Target for Alzheimer's Disease. *Current Alzheimer Research*, *13*(10), 1173–1177. https://doi.org/10.2174/1567205013666160404120542

Duce, J. A., Zhu, X., Jacobson, L. H., & Beart, P. M. (2019). Therapeutics for dementia and Alzheimer's disease: New directions for precision medicine. *British Journal of Pharmacology*, *176*(18), 3409–3412. https://doi.org/10.1111/bph.14767

Durban, J., Sanz, L., Trevisan-Silva, D., Neri-Castro, E., Alagón, A., & Calvete, J. J. (2017). Integrated Venomics and Venom Gland Transcriptome Analysis of Juvenile and Adult Mexican Rattlesnakes *Crotalus simus*, *C. tzabcan* , and *C. culminatus* Revealed miRNA-modulated Ontogenetic Shifts. *Journal of Proteome Research*, *16*(9), 3370–3390. https://doi.org/10.1021/acs.jproteome.7b00414

Ferreira De Oliveira, N., Sachetto, A. T. A., & Santoro, M. L. (2022). Two-Dimensional Blue Native/SDS Polyacrylamide Gel Electrophoresis for Analysis of Brazilian Bothrops Snake Venoms. *Toxins*, *14*(10), 661. https://doi.org/10.3390/toxins14100661

Ferreira-Vieira, T. H., Guimaraes, I. M., Silva, F. R., & Ribeiro, F. M. (2016). Alzheimer's disease: Targeting the Cholinergic System. *Current Neuropharmacology*, *14*(1), 101–115. https://doi.org/10.2174/1570159x13666150716165726

Flores-Holguín, N., Frau, J., & Glossman-Mitnik, D. (2021). In Silico Pharmacokinetics, ADMET Study and Conceptual DFT Analysis of Two Plant Cyclopeptides Isolated From Rosaceae as a Computational Peptidology Approach. *Frontiers in Chemistry*, *9*, 708364. https://doi.org/10.3389/fchem.2021.708364

Frimayanti, N., Yaeghoobi, M., Ikhtiarudin, I., Putri, D. R. W., Namavar, H., & Bitaraf, F. S. (2021). Insight on the in silico study and biological activity assay of chalcone-based 1, 5-benzothiazepines as potential inhibitor for breast cancer MCF7. *Natural and Life Sciences Communications*, *20*(1), e2021019.

Fry, B. G., Vidal, N., Norman, J. A., Vonk, F. J., Scheib, H., Ramjan, S. F. R., Kuruppu, S., Fung, K., Blair Hedges, S., Richardson, M. K., Hodgson, Wayne. C., Ignjatovic, V., Summerhayes, R., & Kochva, E. (2006). Early evolution of the venom system in lizards and snakes. *Molecular & Cellular Proteomics*, *439*(7076), 584–588. https://doi.org/10.1038/nature04328

Greig, N. H., Utsuki, T., Ingram, D. K., Wang, Y., Pepeu, G., Scali, C., Yu, Q.-S., Mamczarz, J., Holloway, H. W., Giordano, T., Chen, D., Furukawa, K., Sambamurti, K., Brossi, A., & Lahiri, D. K. (2005). Selective butyrylcholinesterase inhibition elevates brain acetylcholine, augments learning and lowers Alzheimer β-amyloid peptide in rodent. *Proceedings of the National Academy of Sciences*, *102*(47), 17213–17218. https://doi.org/10.1073/pnas.0508575102

Hidayatullah, A., Putra, W. E., Salma, W. O., Muchtaromah, B., Permatasari, G. W., Susanto, H., Widiastuti, D., & Kismurtono, M. (2020). Discovery of Drug Candidate from Various Natural Products as Potential Novel Dengue Virus Nonstructural Protein 5 (NS5) Inhibitor. *Chiang Mai University Journal of Natural Sciences*, *20*(1). https://doi.org/10.12982/CMUJNS.2021.018

Hill, R. E., & Mackessy, S. P. (1997). Venom yields from several species of colubrid snakes and differential effects of ketamine. *Toxicon*, *35*(5), 671–678. https://doi.org/10.1016/S0041-0101(96)00174-2

Jovičić, S. M. (2024). Enzyme ChE, cholinergic therapy and molecular docking: Significant considerations and future perspectives. *International Journal of Immunopathology and Pharmacology*, *38*, 03946320241289013. https://doi.org/10.1177/03946320241289013

Kandiah, N., Pai, M.-C., Senanarong, V., Looi, I., Ampil, E., Park, K. W., Karanam, A. K., & Christopher, S. (2017). Rivastigmine: The advantages of dual inhibition of acetylcholinesterase and butyrylcholinesterase and its role in subcortical vascular dementia and Parkinson’s disease dementia. *Clinical Interventions in Aging*, *Volume 12*, 697–707. https://doi.org/10.2147/CIA.S129145

Karlsson, E., Mbugua, P. M., & Rodriguez-Ithurralde, D. (1984). Fasciculins, anticholinesterase toxins from the venom of the green mamba Dendroaspis angusticeps. *Journal De Physiologie*, *79*(4), 232–240.

Khimmaktong, W., Nuanyaem, N., Lorthong, N., Hodgson, W. C., & Chaisakul, J. (2022). Histopathological Changes in the Liver, Heart and Kidneys Following Malayan Pit Viper (Calloselasma rhodostoma) Envenoming and the Neutralising Effects of Hemato Polyvalent Snake Antivenom. *Toxins*, *14*(9), 601. https://doi.org/10.3390/toxins14090601

Kusuma, W. A., Fadli, A., Fatriani, R., Sofyantoro, F., Yudha, D. S., Lischer, K., Nuringtyas, T. R., Putri, W. A., Purwestri, Y. A., & Swasono, R. T. (2023). Prediction of the interaction between Calloselasma rhodostoma venom-derived peptides and cancer-associated hub proteins: A computational study. *Heliyon*, *9*(11), e21149. https://doi.org/10.1016/j.heliyon.2023.e21149

Lai, R., & Lu, Q. (2023). Advanced Research on Animal Venoms in China. *Toxins*, *15*(4), 272. https://doi.org/10.3390/toxins15040272

Lee, S., Youn, K., Lim, G., Lee, J., & Jun, M. (2018). In Silico Docking and In Vitro Approaches towards BACE1 and Cholinesterases Inhibitory Effect of Citrus Flavanones. *Molecules*, *23*(7), 1509. https://doi.org/10.3390/molecules23071509

Li, S., Li, A. J., Travers, J., Xu, T., Sakamuru, S., Klumpp-Thomas, C., Huang, R., & Xia, M. (2021). Identification of Compounds for Butyrylcholinesterase Inhibition. *SLAS Discovery: Advancing Life Sciences R & D*, *26*(10), 1355–1364. https://doi.org/10.1177/24725552211030897

Liao, Y., Mai, X., Wu, X., Hu, X., Luo, X., & Zhang, G. (2022). Exploring the Inhibition of Quercetin on Acetylcholinesterase by Multispectroscopic and In Silico Approaches and Evaluation of Its Neuroprotective Effects on PC12 Cells. *Molecules*, *27*(22), 7971. https://doi.org/10.3390/molecules27227971

Liesener, A., Perchuc, A.-M., Schöni, R., Schebb, N. H., Wilmer, M., & Karst, U. (2007). Screening of acetylcholinesterase inhibitors in snake venom by electrospray mass spectrometry. *Pure and Applied Chemistry*, *79*(12), 2339–2349. https://doi.org/10.1351/pac200779122339

Lu, S.-H., Wu, J. W., Liu, H.-L., Zhao, J.-H., Liu, K.-T., Chuang, C.-K., Lin, H.-Y., Tsai, W.-B., & Ho, Y. (2011). The discovery of potential acetylcholinesterase inhibitors: A combination of pharmacophore modeling, virtual screening, and molecular docking studies. *Journal of Biomedical Science*, *18*(1), 8. https://doi.org/10.1186/1423-0127-18-8

Ma, C., Hong, F., & Yang, S. (2022). Amyloidosis in Alzheimer's Disease: Pathogeny, Etiology, and Related Therapeutic Directions. *Molecules (Basel, Switzerland)*, *27*(4), 1210. https://doi.org/10.3390/molecules27041210

Makin, S. (2018). The amyloid hypothesis on trial. *Nature*, *559*(7715), S4–S7. https://doi.org/10.1038/d41586-018-05719-4

Monteiro, A. R., Barbosa, D. J., Remião, F., & Silva, R. (2023). Alzheimer's disease: Insights and new prospects in disease pathophysiology, biomarkers and disease-modifying drugs. *Biochemical Pharmacology*, *211*, 115522. https://doi.org/10.1016/j.bcp.2023.115522

Mughal, E. U., Sadiq, A., Ayub, M., Naeem, N., Javid, A., Sumrra, S. H., Zafar, M. N., Khan, B. A., Malik, F. P., & Ahmed, I. (2021). Exploring 3-Benzyloxyflavones as new lead cholinesterase inhibitors: Synthesis, structure–activity relationship and molecular modelling simulations. *Journal of Biomolecular Structure and Dynamics*, *39*(16), 6154–6167. https://doi.org/10.1080/07391102.2020.1803136

Mushtaq, G., Greig, N., Khan, J., & Kamal, M. (2014). Status of Acetylcholinesterase and Butyrylcholinesterase in Alzheimer's Disease and Type 2 Diabetes Mellitus. *CNS & Neurological Disorders - Drug Targets*, *13*(8), 1432–1439. https://doi.org/10.2174/1871527313666141023141545

Neumann, C., Slagboom, J., Somsen, G. W., Vonk, F., Casewell, N. R., Cardoso, C. L., & Kool, J. (2020). Development of a generic high-throughput screening assay for profiling snake venom protease activity after high-resolution chromatographic fractionation. *Toxicon*, *178*, 61–68. https://doi.org/10.1016/j.toxicon.2020.02.015

Nordberg, A., Darreh-Shori, T., Peskind, E., Soininen, H., Mousavi, M., Eagle, G., & Lane, R. (2009). Different Cholinesterase Inhibitor Effects on CSF Cholinesterases in Alzheimer Patients. *Current Alzheimer Research*, *6*(1), 4–14. https://doi.org/10.2174/156720509787313961

Obaid, R. J., Mughal, E. U., Naeem, N., Al-Rooqi, M. M., Sadiq, A., Jassas, R. S., Moussa, Z., & Ahmed, S. A. (2022). Pharmacological significance of nitrogen-containing five and six-membered heterocyclic scaffolds as potent cholinesterase inhibitors for drug discovery. *Process Biochemistry*, *120*, 250–259. https://doi.org/10.1016/j.procbio.2022.06.009

Obaid, R. J., Naeem, N., Mughal, E. U., Al-Rooqi, M. M., Sadiq, A., Jassas, R. S., Moussa, Z., & Ahmed, S. A. (2022). Inhibitory potential of nitrogen, oxygen and sulfur containing heterocyclic scaffolds against acetylcholinesterase and butyrylcholinesterase. *RSC Advances*, *12*(31), 19764–19855. https://doi.org/10.1039/D2RA03081K

Oh, A. M. F., Tan, K. Y., Tan, N. H., & Tan, C. H. (2021). Proteomics and neutralization of Bungarus multicinctus (Many-banded Krait) venom: Intra-specific comparisons between specimens from China and Taiwan. *Comparative Biochemistry and Physiology Part C: Toxicology & Pharmacology*, *247*, 109063. https://doi.org/10.1016/j.cbpc.2021.109063

Oliveira, A. L., Viegas, M. F., Da Silva, S. L., Soares, A. M., Ramos, M. J., & Fernandes, P. A. (2022). The chemistry of snake venom and its medicinal potential. *Nature Reviews Chemistry*, *6*(7), 451–469. https://doi.org/10.1038/s41570-022-00393-7

Panachamnong, N., Methapatara, P., Sungkarat, S., Taneyhill, K., & Intasai, N. (2014). Clusterin as a blood biomarker for diagnosis of mild cognitive impairment and Alzheimer's disease. *Natural and Life Sciences Communications*, *13*(3), 331–344.

Peitzika, S.-C., & Pontiki, E. (2023). A Review on Recent Approaches on Molecular Docking Studies of Novel Compounds Targeting Acetylcholinesterase in Alzheimer Disease. *Molecules*, *28*(3), 1084. https://doi.org/10.3390/molecules28031084

Pereira, G. R. C., Gonçalves, L. M., Abrahim-Vieira, B. de A., & De Mesquita, J. F. (2022). In silico analyses of acetylcholinesterase (AChE) and its genetic variants in interaction with the anti-Alzheimer drug Rivastigmine. *Journal of Cellular Biochemistry*, *123*(7), 1259–1277. https://doi.org/10.1002/jcb.30277

Sarkar, B., Alam, S., Rajib, T. K., Islam, S. S., Araf, Y., & Ullah, Md. A. (2021). Identification of the most potent acetylcholinesterase inhibitors from plants for possible treatment of Alzheimer's disease: A computational approach. *Egyptian Journal of Medical Human Genetics*, *22*(1), 10. https://doi.org/10.1186/s43042-020-00127-8

Sofyantoro, F., Septriani, N. I., Yudha, D. S., Wicaksono, E. A., Priyono, D. S., Putri, W. A., Primahesa, A., Raharjeng, A. R. P., Purwestri, Y. A., & Nuringtyas, T. R. (2024). Zebrafish as Versatile Model for Assessing Animal Venoms and Toxins: Current Applications and Future Prospects. *Zebrafish*, zeb.2023.0088. https://doi.org/10.1089/zeb.2023.0088

Sofyantoro, F., Yudha, D. S., Lischer, K., Nuringtyas, T. R., Putri, W. A., Kusuma, W. A., Purwestri, Y. A., & Swasono, R. T. (2022). Bibliometric analysis of literature in snake venom-related research worldwide (1933–2022). *Animals*, *12*(16), 2058. https://doi.org/10.3390/ani12162058

Stern, N., Gacs, A., Tátrai, E., Flachner, B., Hajdú, I., Dobi, K., Bágyi, I., Dormán, G., Lőrincz, Z., Cseh, S., Kígyós, A., Tóvári, J., & Goldblum, A. (2022). Dual Inhibitors of AChE and BACE-1 for Reducing Aβ in Alzheimer's Disease: From In Silico to In Vivo. *International Journal of Molecular Sciences*, *23*(21), 13098. https://doi.org/10.3390/ijms232113098

Tan, K. Y., Shamsuddin, N. N., & Tan, C. H. (2022). Sharp-nosed Pit Viper (Deinagkistrodon acutus) from Taiwan and China: A comparative study on venom toxicity and neutralization by two specific antivenoms across the Strait. *Acta Tropica*, *232*, 106495. https://doi.org/10.1016/j.actatropica.2022.106495

Tang, E. L. H., Tan, C. H., Fung, S. Y., & Tan, N. H. (2016). Venomics of Calloselasma rhodostoma , the Malayan pit viper: A complex toxin arsenal unraveled. *Journal of Proteomics*, *148*, 44–56. https://doi.org/10.1016/j.jprot.2016.07.006

Tang, E. L. H., Tan, N. H., Fung, S. Y., & Tan, C. H. (2019). Comparative proteomes, immunoreactivities and neutralization of procoagulant activities of Calloselasma rhodostoma (Malayan pit viper) venoms from four regions in Southeast Asia. *Toxicon*, *169*, 91–102. https://doi.org/10.1016/j.toxicon.2019.08.004

van der Schaar, J., Visser, L. N. C., Bouwman, F. H., Ket, J. C. F., Scheltens, P., Bredenoord, A. L., & van der Flier, W. M. (2022). Considerations regarding a diagnosis of Alzheimer's disease before dementia: A systematic review. *Alzheimer's Research & Therapy*, *14*(1), 31. https://doi.org/10.1186/s13195-022-00971-3

Vejayan, J., Shin Yee, L., Ponnudurai, G., Ambu, S., & Ibrahim, I. (2010). Protein profile analysis of Malaysian snake venoms by two-dimensional gel electrophoresis. *Journal of Venomous Animals and Toxins Including Tropical Diseases*, *16*(4), 623–630. https://doi.org/10.1590/S1678-91992010000400013

Wright, C. I., Geula, C., & Mesulam, M. -Marsel. (1993). Neuroglial cholinesterases in the normal brain and in Alzheimer's disease: Relationship to plaques, tangles, and patterns of selective vulnerability. *Annals of Neurology*, *34*(3), 373–384. https://doi.org/10.1002/ana.410340312

Xing, S., Li, Q., Xiong, B., Chen, Y., Feng, F., Liu, W., & Sun, H. (2021). Structure and therapeutic uses of butyrylcholinesterase: Application in detoxification, Alzheimer's disease, and fat metabolism. *Medicinal Research Reviews*, *41*(2), 858–901. https://doi.org/10.1002/med.21745

Xiong, G., Wu, Z., Yi, J., Fu, L., Yang, Z., Hsieh, C., Yin, M., Zeng, X., Wu, C., Lu, A., Chen, X., Hou, T., & Cao, D. (2021). ADMETlab 2.0: An integrated online platform for accurate and comprehensive predictions of ADMET properties. *Nucleic Acids Research*, *49*(W1), W5–W14. https://doi.org/10.1093/nar/gkab255

APPENDIX

Supplementary Table 1
Composition of proteins within crude C. rhodostoma venom following trypsin-mediated digestion elucidated via LC-HRMS analysis

Protein Family	Protein	Accession Protein	Total Peptide Sequences	Molecular Weight (kDa)
LAAO	L-amino-acid oxidase OS=*Calloselasma rhodostoma*	P81382	31	58,2
	L-amino-acid oxidase OS=*Bungarus fasciatus*	A8QL52	3	58,7
PLA-2	Basic phospholipase A2 homolog W6D49 OS=*Calloselasma rhodostoma*	Q9PVF4	10	15,4
	Acidic phospholipase A2 S1E6-c OS=*Calloselasma rhodostoma*	Q9PVE9	7	15,8
	Phospholipase A2 OS=*Calloselasma rhodostoma*	A0A0H3U266	6	15,5
SVMP	Snake venom metalloproteinase kistomin OS=*Calloselasma rhodostoma*	P0CB14	18	47,4
	Zinc metalloproteinase/disintegrin OS=*Calloselasma rhodostoma*	P30403	11	54
Thrombin like Enzyme ancrod	Thrombin-like enzyme ancrod OS=*Calloselasma rhodostoma*	P26324	10	26,6
	Thrombin-like enzyme ancrod-2 OS=*Calloselasma rhodostoma*	P47797	4	29,1
Snaclec/ CTL	Snaclec rhodocetin subunit alpha OS=*Calloselasma rhodostoma*	P81397	12	16
	Snaclec rhodocetin subunit beta OS=*Calloselasma rhodostoma*	P81398	6	15,2
	Snaclec rhodocetin subunit delta OS=*Calloselasma rhodostoma*	D2YW40	5	14,8
	Snaclec rhodocetin subunit gamma (Fragment) OS=*Calloselasma rhodostoma*	D2YW39	5	15,7
	Snaclec rhodocytin subunit alpha OS=*Calloselasma rhodostoma*	Q9I841	5	15,8
	Snaclec rhodocytin subunit beta OS=*Calloselasma rhodostoma*	Q9I840	3	16,8

Supplementary Table 2
Peptide sequences identified in the crude venom of C. rhodostoma following trypsin digestion, analyzed via Liquid Chromatography-High Resolution Mass Spectrometry (LC-HRMS)

No	Master Protein	Sequence
1.	L-amino-acid oxidase	NEEAGWYANLGPMR
		RFDEIVDGMDKLPTAMYR
		KDIQSFCYPSVIQK
		VTVVYETLSK
		SAGQLYEESLGK
		RFDEIVDGMDK
		FDEIVDGMDKLPTAMYR
		ETPSVTADYVIVCTTSR
		EGDLSPGAVDMIGDLLNEDSGYYVSFIESLKHDDIFAYEK
		NPLAECFQENDYEEFLEIAR
		DCADIVFNDLSLIHQLPK
		HVVIVGAGMAGLSAAYVLAGAGHQVTVLEASERPGGR
		EGDLSPGAVDMIGDLLNEDSGYYVSFIESLK
		NEEAGWYANLGPMRLPEK
		DIQSFCYPSVIQK
		LNEFSQENDNAWYFIK
		HDDIFAYEK
		EGDLSPGAVDMIGDLLNEDSGYYVSFIESLK
		IFLTCTTK
		KDPGLLK
		YDTYSTK
		STTDLPSR
		FDEIVDGMDK
		FWEDDGIHGGK
		KVGEVK
		VHFNAQVIK
		DPGLLK
		VVEELK
		FNPPLLPK
		LPTAMYR
		LIKFNPPLLPK
2.	Snake venom metalloproteinase kistomin	VYLVIVADKSMVDK
		ETLYSFAK
		SSAKETLYSFAK
		WRVEDLSK
		IEEQGHQMVNTMNECYRPMGIIIIMAGIECWTTNDFFEVK
		DFDGNTVGLAFVGGICNEK
		DFDGNTVGLAFVGGICNEKYCAGVVQDHTK
		VPLLMAITMGHEIGHNLGMEHDEANCK

Supplementary Table 2 *(continue)*

No	Master Protein	Sequence
		ACVMAPEVNNNPTKK
		DRKPECLFK
		KPECLFK
		KPHNDAQFLTNK
		ACVMAPEVNNNPTK
		YCAGVVQDHTK
		SMVDKHNGNIK
		VEDLSK
		ACVMAPEVNNNPTK
		VYLVIVADK
3.	Zinc metalloproteinase/ disintegrin	AYLDSICDPER
		YIENQNPQCILNKPLR
		HVDIVVVVDSR
		HDGEYCTCYGSSECIMSSHISDPPSK
		SVGIVQNYHGITLNVAAIMAHEMGHNLGVR
		HSNDLEVIR
		ESDLIK
		LRPGAQCGEGLCCEQCK
		GDMPDDR
		CTGQSADCPR
		ECDCSSPENPCCDAATCK
4.	Snaclec rhodocetin subunit alpha	CFLMDHQSGLPK
		SWIGLK
		LEAVFVDMVMENNFENK
		SNLEWSDGSSISYENLYEPYMEK
		TWEEAER
		DCPDGWSSTK
		EAHLVSMENR
		FCTEQEKEAHLVSMENR
		WHTADCEEK
		CFLMDHQSGLPK
		NVFMCK
		FCTEQEK
5.	Thrombin-like enzyme ancrod	GPNPCAQPNKPALYTSIYDYR
		IDVLSDEPR
		DSCNSDSGGPLICNEELHGIVAR
		TSWDEDIMLIR
		FDDEQERYPK
		VIGGDECNINEHR
		FDDEQER

Supplementary Table 2 *(continue)*

No	Master Protein	Sequence
		RIDVLSDEPR
		SEKFDDEQERYPK
		VLCAGDLR
6.	Basic phospholipase A2 homolog	QQFNTGIFCSK
		GEILCGETNPCLNQACECDK
		FEKGEILCGETNPCLNQACECDK
		DNLDTYNKK
		DATDQCCADHDCCYK
		NYGMYGCNCGPMK
		MIMVMTGK
		KLTDCDPK
		ESYSYK
		DNLDTYNK
7.	Acidic phospholipase A2	TATYSYTEENDGIVCGGDDPCK
		TATYSYTEENDGIVCGGDDPCKK
		SGFFWYSFYGCYCGWGGHGLPQDPTDR
		RSGFFWYSFYGCYCGWGGHGLPQDPTDR
		CCFVHDCCYGK
		QVCECDR
		CQEDPEPC
8.	Phospholipase A2	FNTGIFCSK
		GEILCGETNPCLNQACECDK
		FEKGEILCGETNPCLNQACECDK
		NYGMYGCNCGPMK
		MIMVMTGK
		ESYSYK
9.	Snaclec rhodocytin subunit alpha	AQENGAHLASIESNGEADFVSWLISQK
		DELADEDYVWIGLR
		GLEDCDFGWSPYDQHCYQAFNEQK
		EQQCSSEWSDGSSVSYENLIDLHTK
		TWDEAEK
10.	Thrombin-like enzyme ancrod-2	LDSCHCDSGGPLICSEEFHGIVYR
		YIDVLPDEPR
		FDDEQER
		FDDEQERFPK
11.	Snaclec rhodocetin subunit beta	CFVVQPWEGK
		QAENGHLVSIGSAAEADFLDLVIVVNFDK
		NAFLCK
		CPTTWSASK
		TWIEAER
		AWTGLTER

Supplementary Table 2 *(continue)*

No	Master Protein	Sequence
12.	Snaclec rhodocetin subunit delta	TWEDAESFCYAQHK EEEAFVGK TVSFVCK RPYCAVMVVK WEWSDDAK
13.	Snaclec rhodocetin subunit gamma (Fragment)	GHLVSIGSDGEADFVAQLVTNNIK DFNCLPGWSAYDQHCYQAFNEPK TWDEAER WDYSDCQAK NPFVCK
14.	Snaclec rhodocytin subunit beta	DWQEQSECLAFR GVHTEWLNMDCSSTCSFVCK NWADAER
15.	L-amino-acid oxidase	YPVKPSEEGK YDTYSTK STTDLPSR

Supplementary Table 3
Characterization of proteins elicited from Anion Exchange Chromatography fractionation of C. rhodostoma venom via trypsin digestion and analyzed by LC-HRMS

Protein Family	Protein	Accession Protein	Total Peptide Sequences	Molecular Weight (kDa)
SVMP	Snake venom metalloproteinase kistomin	P0CB14	2	47,4
	Zinc metalloproteinase atau disintegrin	P30403	8	54
PLA-2	Basic phospholipase A2 homolog	Q9PVF4	2	15,4
Thrombin-like Enzyme Ancrod	Thrombin-like enzyme ancrod	P26324	10	26,6
	Thrombin-like enzyme ancrod-2	P47797	3	29,1
Snaclec atau CTL	Snaclec rhodocetin subunit alpha	P81397	6	16
	Snaclec rhodocetin subunit beta	P81398	6	15,2
	Snaclec rhodocetin subunit delta	D2YW40	3	14,8
	Snaclec rhodocytin subunit alpha	Q9I841	1	15,8
	Snaclec rhodocetin subunit gamma	D2YW39	1	15,7

Supplementary Table 4
Peptide sequences identified from the Anion Exchange Chromatography fraction of C. rhodostoma following trypsin digestion analyzed by LC-HRMS

No	Master Protein	Sequence
1	Zinc metalloproteinase/ disintegrin	LRPGAQCGEGLCCEQCK HDGEYCTCYGSSECIMSSHISDPPSK

Supplementary Table 4 *(continue)*

No	Master Protein	Sequence
		ECDCSSPENPCCDAATCK HVDIVVVVDSR HSNDLEVIR
2	Thrombin-like enzyme ancrod	CTGQSADCPR YIENQNPQCILNKPLR AYLDSICDPER DSCNSDSGGPLICNEELHGIVAR VIGGDECNINEHR RIDVLSDEPR TSWDEDIMLIR IDVLSDEPR MNLVFGMHR FDDEQERYPK FDDEQER VLCAGDLR
3	Snaclec rhodocetin subunit alpha	VMGWGSINR LEAVFVDMVMENNFENK CFLMDHQSGLPK EAHLVSMENR DCPDGWSSTK TWEEAER
4	Snaclec rhodocetin subunit beta	SWIGLK CFVVQPWEGK CPTTWSASK KCFVVQPWEGK TWIEAER AWTGLTER KTWIEAER
5	Snake venom metalloproteinase kistomin	IEEQGHQMVNTMNECYRPMGIIIIMAGIECWTTNDFFEVK DFDGNTVGLAFVGGICNEK
6	Basic phospholipase A2 homolog W6D49	GEILCGETNPCLNQACECDK QQFNTGIFCSK
7	Snaclec rhodocetin subunit delta	TWEDAESFCYAQHK WEWSDDAK
8	Thrombin-like enzyme ancrod-2	LASQTLK ILCAGDLQGR FDDEQER YIDVLPDEPR
9	Snaclec rhodocytin subunit alpha	DELADEDYVWIGLR
10	Snaclec rhodocetin subunit gamma (Fragment)	WDYSDCQAK